Controlled Growth of Silica Shell on $Ba_{0.6}Sr_{0.4}TiO_3$ Nanoparticles Used As Precursors of Ferroelectric Composites

S. Mornet,*[,†,‡] C. Elissalde,[†] V. Hornebecq,[§] O. Bidault,[†] E. Duguet,[†] A. Brisson,[‡] and M. Maglione[†]

Institut de Chimie de la Matière Condensée de Bordeaux, ICMCB UPR CNRS 9048, Université Bordeaux-1, 87 Avenue du Dr A. Schweitzer, F-33608 Pessac Cedex, France, Molecular Imaging and Nano-Bio-Technology, IECB UMR CNRS 5471, Université Bordeaux-1, 2 rue Robert Escarpit, F-33607 Pessac, France, and Matériaux Divisés, Revêtements et Electrocéramiques, MADIREL UMR CNRS 6121, Université de Provence, Centre de Saint Jérôme, F-13397 Marseille Cedex, France

Received April 26, 2005. Revised Manuscript Received June 21, 2005

A method based on a seeded growth process was developed to coat ferroelectric nanoparticles with a dielectric silica shell. This method, applied to size-polydispersed $(Ba_{0.6}Sr_{0.4})TiO_3$ particles (BST, mean diameter 150 nm), allows the control of the silica shell thickness from 2 to 80 nm with an accuracy of 1−2 nm. The morphology and surface physical chemistry of the core−shell were studied by transmission electron microscopy, photon correlation spectroscopy, and zeta potential measurements. A size-sorting procedure consisting of several cycles of centrifugation was optimized to extract the BST@silica nanoparticles of the required size for dielectric properties tuning. Upon sintering, dielectric measurements showed that the ferroelectric transition was maintained in the dense nanocomposites.

Introduction

The use of silica as a coating material has a long tradition in colloid science because it is a smart way to give any particle the impressive stability of silica sols over a wide range of polar and nonpolar solvents. In particular, aqueous dispersions of silica may be stabilized in a large pH range due to its low isoelectric point (IEP at pH 2). Intrinsic properties of silica are also of a great interest: chemical inertness, thermal stability, optical transparency, tunable porosity, and ability to be easily surface-modified, especially by silane derivatives. Therefore, silica coating is widely used to prepare functional nanomaterials with tailored properties. As an example, it allows tuning of the optical properties of metallic or semiconducting (quantum dots) particles.[1−3] Moreover, the interaction potential can be changed, leading to 2-D and 3-D ordering of colloidal self-assemblies for photonic crystals,[1] composite material porosity tailoring,[2] surfaces structuring at the nanometer scale,[4] etc. Core−shell nanoparticles, like crystal unit cells, can be used as bricks for bottom-up approaches, and to that extent as carriers for biomedical purposes. Silica-coated magnetite and quantum dots nanoparticles have been used for bioseparation processes[5] and as biomarkers.[6,7] An outer silica shell can be used as a substrate with high affinity to adsorb biological molecules such as oligonucleotides for DNA hybridization[8] or phospholipid bilayers for biomimetic membrane devices.[9]

The material requirements for processing agile high-frequency devices, such as tunable resonators or phase shifters, are low dielectric losses (≪1%), relatively high permittivity values ($\epsilon_r' > 100$), and a significant electric field dependence of the permittivity. That is the reason composite materials including ferroelectric fillers, such as $(Ba_{0.6}Sr_{0.4})TiO_3$ (BST), dispersed in dielectric matrixes based on low losses oxides, are very promising candidates for telecommunication devices. In our pioneering work, we apply the core−shell concept to ferroelectric nanoparticles in which the BST core was surrounded by a silica shell, as low loss dielectric oxide.[10] This was done to overcome the limitations found using the solid-state route to synthesize composites.[11−14] Indeed, in such a case, the properties improvement is limited due to interdiffusion evidenced between the two phases. With use of the core−shell concept, the efficiency of the coating was checked. However, the process used was based on sodium metasilicate synthesis and does not allow, as revealed by transmission electron microscopy (TEM) images, a continuous and homogeneous coating. As a result, the contact between ferroelectric cores was hardly avoided during the

* To whom correspondence should be addressed. E-mail: mornet@icmcb-bordeaux.cnrs.fr. Tel.: +33 5 40003487. Fax: +33 5 40003484.
† ICMCB UPR CNRS 9048, Université Bordeaux-1.
‡ IECB UMR CNRS 5471, Université Bordeaux-1.
§ MADIREL UMR CNRS 6121, Université de Provence.

(1) Liz-Marzan, L. M.; Mulvaney, P. J. *Phys. Chem. B* **2003**, *107*, 7312.
(2) Wang, D.; Caruso, R. A.; Caruso, F. *Chem Mater.* **2001**, *13*, 364.
(3) Rogach, A. L.; Nagesha, D.; Ostrander, J. W.; Giersig, M.; Kotov, N. A. *Chem. Mater.* **2000**, *12*, 2676.
(4) Xia, D.; Brueck, S. R. J. *Nano Lett.* **2004**, *4*, 1295.
(5) Yang, H.-H.; Zhang, S.-Q.; Chen, X.-L.; Zhuang, Z.-X.; Xu, J.-G.; Wang, X.-R. *Anal. Chem.* **2004**, *76*, 1316.
(6) Bruchez, M., Jr.; Moronne, M.; Gin, P.; Weiss, S.; Alivisatos, A. P. *Science* **1998**, *281*, 2013.
(7) Santra, S.; Zhang, P.; Wang, K.; Tapec, R.; Tan, W. *Anal. Chem.* **2001**, *73*, 4988.
(8) Hilliard, L. R.; Zhao, X.; Tan, W. *Anal. Chim. Acta* **2002**, *470*, 51.
(9) Mornet, S.; Lambert, O.; Duguet, E.; Brisson, A. *Nano Lett.* **2005**, *5*, 281.
(10) Huber, C.; Treguer-Delapierre, M.; Elissalde, C.; Weill, F.; Maglione, M. *J. Mater. Chem.* **2003**, *13*, 1.
(11) Alberta, E. F.; Guo, R.; Bhalla, A. S.; Pardo, L.; Jimenez, R. *Ferroelectrics* **2002**, *268*, 169.
(12) Sengupta, L. C. U.S. Patent No. 5,635,434, 1997.
(13) Chin, L.; Zhang, X.; Sengupta, L. C. U.S. Patent No. 6,514,895, 2003.
(14) Sengupta, L. C.; Sengupta, S. U.S. Patent No. 663,719, 2000.

10.1021/cm050884r CCC: $30.25
Published on Web 07/23/2005

sintering step. That is the reason we investigated a new coating route, susceptible to coat perfectly BST nanoparticles, to tune the silica shell thickness on a wider range, and then to obtain a final composite with the required dielectric properties.

In the present paper, we report on the stabilization of BST nanoparticles in the ethanol/ammonia medium, the successful coating by silica shell from a few nanometers up to 80 nm, and the size-sorting procedure developed for narrowing the size polydispersity of the pristine BST cores. These results are supported by TEM, zeta potential vs pH measurements, and hydrodynamic size-distribution curves as determined by photon correlation spectroscopy (PCS). We also investigate, using scanning electron microscopy and dielectric measurements, the influence of the characteristics of the green powder on the microstructure and dielectric properties of the obtained ceramics.

Experimental Section

Materials. $Ba_{0.6}Sr_{0.4}TiO_3$ (BST) nanoparticles of mean diameter close to 50 nm were purchased from Pi-Kem (Shropshire, England). Starting from 50 nm BST powder, samples were pressed into disks and annealed at 1100 °C for 2 h with a heating rate of 200 °C/h under an oxygen atmosphere to increase the average grain size up to 150 nm. Tetraethoxysilane (TEOS) (98+%) and citric acid (99.5+%) were purchased from Aldrich. Absolute ethanol (J.T. Baker) and ammonia (Carlo Erba) were used as received. All other reagents were of analytical grade. Water was deionized (resistivity higher than 18 MΩ). Sample powders were recovered by centrifugation using a Jouan BB 3V apparatus (Saint Herblain, France).

Synthesis of BST@silica Nanoparticles. The new selected method was derived from the so-called Stöber process widely used for the synthesis of silica beads from a few tens to a few hundreds of nanometers.[15,16] It was based on the hydrolysis/condensation of tetraethoxysilane (TEOS) catalyzed by ammonia in alcoholic media. The surface of BST nanoparticles was activated by acidic treatment: 500 mg of BST was placed in a sonicator bath for 15 min in 10 mL of 1 M HNO_3. After removal of the supernatant by centrifugation at 2500*g* for 5 min and washing of the pellet in the same volume of deionized water, the particles were redispersed in 10 mL of 0.01 M citric acid. They were again sonicated and centrifuged in the same conditions. The pellet was dispersed in 20 mL of water and peptization was performed by adding 20 μL of ammonia. Then, the alkaline sol of citrated-BST nanoparticles was poured in 100 mL of ethanol−water−ammonia solution 75/23.5/1.5 v/v/v %. To tune the silica shell thickness, the amount of TEOS to be added was calculated from the initial and final particle size, taking into account the number N_{pBST} of BST nanoparticles, by means of the following formula:

$$V_{TEOS} = 3.89 N_{pBST} (D^3 - d^3) \quad (1)$$

where V_{TEOS} is directly expressed in mL if D and d are the final and the starting diameter expressed in centimeters. The 3.89 scaling factor was computed from the molecular weights of SiO_2 formula unit and TEOS, the densities of silica, TEOS, and BST (2 g/cm^3, 0.934 g/cm^3, and 5.6 g/cm^3, respectively), and the assumption that BST nanoparticles are spherical.

Size Sorting of BST@silica Nanoparticles. To extract the main size population of coated nanoparticles, many cycles of centrifugation were carried out. The first step consists of sorting the largest sub-micrometer particles by low-speed centrifugation (1200*g* for 3 min). The supernatant was recovered and centrifuged again in order to remove the smallest ones (2500*g* for 10 min). The pellet was then redispersed in ultrapure water with the aid of an ultrasound bath for 10 min. This operation was repeated twice. In the last operation, the pellet was recovered and dried at 100 °C on air.

Characterizations. Core−shell morphologies were investigated by TEM. Samples were ground in agate mortar and suspended in ethanol. Drops of diluted dispersions were air-dried on carbon films deposited on 200-mesh copper grids. The excess liquid was blotted with filter paper. TEM images were recorded using a Philips EM 120 electron microscope operating at 120 kV. The average thickness of silica shells was determined from these images by measurements in four directions for each particle and at least 50 particles per BST@silica sample.

Zeta potential and mean hydrodynamic diameters of BST and BST@silica nanoparticles were assessed by using a Zetasizer 3000HSA setup (Malvern Instruments) equipped with a He−Ne laser (50 mW, 532 nm). The zeta potential measurement based on laser Doppler interferometry was used to assess the electrophoretic mobility of nanoparticles. Measurements were performed for 20 s using a standard capillary electrophoresis cell. The dielectric constant of solvent (water) was set to 80.4 and the Smoluchowsky constant $f(ka)$ was 1.5. The hydrodynamic diameter of nanoparticles was determined by PCS with a sample refractive index of 1.59 and a viscosity of 0.89 cP. The given mean diameter is an average size calculated by using the monomodal analysis mode.

The microstructure of the sintered compacts was studied using a scanning electron microscope JEOL JSM 6360A. A thin platinum coating was deposited on the fracture surface prior to observation.

For dielectric evaluation, the major faces of the dense composite compacts were electroded using gold vapor deposition. The composite was then placed in a homemade cell connected to a membrane pump to avoid moisture. The temperature was controlled using a Pt resistor in thermal contact with the sample. The temperature could be monitored between 80 and 450 K with accuracy better than 0.1 K using a temperature controller LakeShore DRC93CA. The dielectric parameters were measured using a HP 4192 impedance analyzer in a frequency range from 100 Hz to 10 MHz. The electrical measurements (conductivity and impedance spectroscopy) were performed using a dynamic method under linear temperature variation (typically ±1 K/min). Such a rate was used in order to avoid a temperature gradient within the sample.

Results and Discussion

The size of the BST cores was chosen considering the size effects in such materials.[17] As a result, the nanomaterials produced with a 150 nm ferroelectric core and a controlled silica shell thickness are expected to have the same ferroelectric phase transition temperature as the bulk pure ferroelectric phase (T_c = 295 K). Since our aim was to obtain dense nanostructured ceramics exhibiting a Curie temperature in the vicinity of room temperature, the size of BST nanoparticles was increased from 50 to 150 nm by thermal treatment as previously reported.[17] The uncoated grain size, as estimated by TEM, exhibits a large distribution (Figure 1a). Since their size sorting by centrifugation was unsuccessful because of their poor colloidal stability in water, we postponed this step after the silica embedding one.

(15) Stöber, W.; Fink, A.; Bohn, E. *J. Colloid Interface Sci.* **1968**, *26*, 62.
(16) Iler, R. K. U.S. Patent No. 2,885,366, 1959.
(17) Hornebecq, V.; Huber, C.; Maglione, M.; Antonietti, M.; Elissalde, C. *Adv. Funct. Mater.* **2004**, *14*, 899.

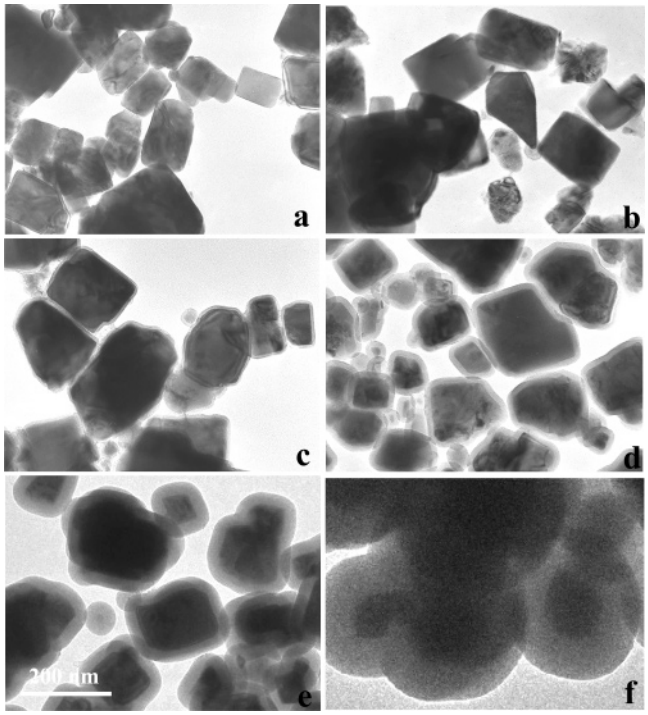

Figure 1. TEM pictures of BST nanoparticles at different stages of the silica shell growth: (a) pristine BST; (b) BST@silica(2); (c) BST@silica-(7); (d) BST@silica(13); (e) BST@silica(25); (f) BST@silica(80). Scale bar is 200 nm for all pictures.

Controlled Growth of Silica Shell. The synthesis of BST@silica nanoparticles is a two-step process: adsorption of citric acid onto pristine BST nanoparticles to help their colloidal stability in the ethanol-based reacting medium and growth of the silica shell through the TEOS hydrolysis/condensation process derived from the Stöber method.

Colloidal Stabilization of BST Nanoparticles. The critical step is the colloidal stabilization of the seeds in the ethanol medium. Clay minerals,[16] hematite,[18] and titania[19] may be readily dispersed and therefore directly coated by silica. But most of the other nanoparticles have to be stabilized in an aqueous medium before being transferred in the ethanol/ammonia media. This is the case of metallic nanoparticles[20−23] (gold, silver, etc.) and of some metallic oxides[23−27] (magnetite, gibbsite, boehmite, etc.), metallic sulfides[28−30] (CdS, ZnS, etc.), and organic[23,31−33] (polystyrene, poly(dimethylsiloxane), etc.) nanoparticles. Stabilizer agents can be macromolecules,[23] chelates,[25] surfactants,[26] or organofunctional polysiloxane primer layers.[20−22]

As has already been reported for $BaTiO_3$,[34,35] $Ba_{0.6}Sr_{0.4}TiO_3$ nanoparticles do not form a stable colloidal suspension in water. If we intend to encapsulate by silica each individual BST nanoparticle, it is necessary to improve first their colloidal stability by modifying their surface. However, the dielectric parameters of the final materials may be disturbed by residual contaminants. Therefore, the chosen stabilizing ligands must have the ability to be easily removed during the washing step. This was achieved by using citric acid. In a first step, BST nanoparticles were pretreated by nitric acid leaching in order to activate the surface sites, to break the bonds between the particles, which had been formed during the previous thermal treatment, and to favor citric acid adsorption. The evolution of zeta potential of pristine and citric acid treated particles was studied as a function of pH to investigate the stability of theses dispersions (Figure 2). The pristine BST suspension displayed two isoelectric points (IEP) at pH 6 and 8.5 with two positive charge zones for pH > 8.5 and pH < 6 (Figure 2a). After treatment by HNO_3, BST suspension exhibits only one IEP equal to 5.1 (Figure 2b), near the one of TiO_2 (i.e., 5.5)[35] or the one of $SrTiO_3$ (i.e., 5.1),[36] suggesting that treated BST are deficient in Ba ions at their surface. Indeed, it is known that barium dissolves at low pH and can act as a potential-determining ion in solution.[34,35] These barium ions, absorbed on the BST surface, change the electrostatic repulsive potential between particles responsible for the dispersion's stability. This explains that pristine BST particles are very difficult to disperse in water. After citric acid adsorption on BST surface, the nanoparticles exhibit an IEP of 4.2 (Figure 2c), around the pK_a values of citric acid (pK_{a1} 3.15; pK_{a2} 4.77) and displays a good stability in an alkaline medium until pH 4.

Coating of Silica Outer Shell, on Top of BST Nanoparticles. To coat the BST particles with silica, TEOS was added in several portions in the dispersion under mild stirring. The total amount of TEOS added was set to comply with the targeted thickness of the silica shell according to eq 1. The first amount of TEOS added (55.5 μL) matches the smallest silica shell thickness of roughly 2 nm (Figure 1b). Then the fitting amount of TEOS was added, after 12 h of reaction, to increase the shell thickness to 6 nm, 15 nm, 25 nm, 40 nm, and so on. In our experiments, the total surface area of BST particles could be estimated around 36 m^2/L for size-polydispersed particles of 75 nm mean radius. In these conditions, no secondary nucleation was observed, which is in agreement with the results of Chen et al.[37] It was observed that the total surface area should be at least about 5 m^2/L for particles of 236 nm radius to prevent a second nucleation. The single isoelectric point of BST@silica-

(18) Ohmori, M.; Matijevic, E. *J. Colloid Interface Sci.* **1992**, *150*, 594.
(19) Ryan, J. N.; Elimelech, M.; Baeseman, J. L.; Magelky, R. D. *Environ. Sci. Technol.* **2000**, *34*, 2000.
(20) Liz-Marzan, L. M.; Giersig, M.; Mulvaney, P. *Langmuir* **1996**, *12*, 4329.
(21) Ung, T.; Liz-Marzan, L. M.; Mulvaney, P. *Langmuir* **1998**, *14*, 3740.
(22) Graf, C.; van Blaaderen, A. *Langmuir* **2002**, *18*, 524.
(23) Graf, C.; Vossen, D. L. J.; Imhof, A.; van Blaaderen, A. *Langmuir* **2003**, *19*, 6693.
(24) Philipse, A. P.; van Bruggen, M. P. B.; Pathmamanoharan, C. *Langmuir* **1994**, *10*, 92.
(25) de Gans, B. J.; Blom, C.; Mellema, J.; Philipse, A. P. *J. Magn. Magn. Mater.* **1999**, *201*, 11.
(26) Mornet, S.; Grasset, F.; Portier, J. *Eur. Cells Mater.* **2002**, *3*, 110.
(27) Santra, S.; Tapec, R.; Theodoropoulou, N.; Bobson, J.; Hebard, A.; Tan, W. *Langmuir* **2001**, *17*, 2900.
(28) Correa-Duarte, M. A.; Giersig, M.; Liz-Marzan, L. M. *Chem. Phys. Lett.* **1998**, *286*, 497.
(29) Velikov, K. P.; van Blaaderen, A. *Langmuir* **2001**, *17*, 4779.
(30) Chang, S.-Y.; Liu, L.; Asher, S. A. *J. Am. Chem. Soc.* **1994**, *116*, 6739.
(31) Goller, M. I.; Vincent, B. *Colloids Surf.* **1998**, *142*, 281.
(32) Lu, Y.; McLellan, J.; Xia, Y. *Langmuir* **2004**, *20*, 3464.
(33) Reculusa, S.; Mingotaud, C.; Bourgeat-Lami, E.; Duguet, E.; Ravaine, S. *Nano Lett.* **2004**, *4*, 1677.
(34) Shih, W.-H.; Kisailus, D.; Wei, Y. *Mater. Lett.* **1995**, *24*, 13.
(35) Chen, Z.-C.; Ring, T. A.; Lemaître, J. *J. Am. Ceram. Soc.* **1992**, *75*, 3201.
(36) Gao, Y.; Masuda, Y.; Koumoto, K. *Chem. Mater.* **2003**, *15*, 2399.
(37) Chen, S.-L.; Dong, P.; Yang, G.-H., Yang, J.-J. *J. Colloid Interface Sci.* **1996**, *180*, 237.

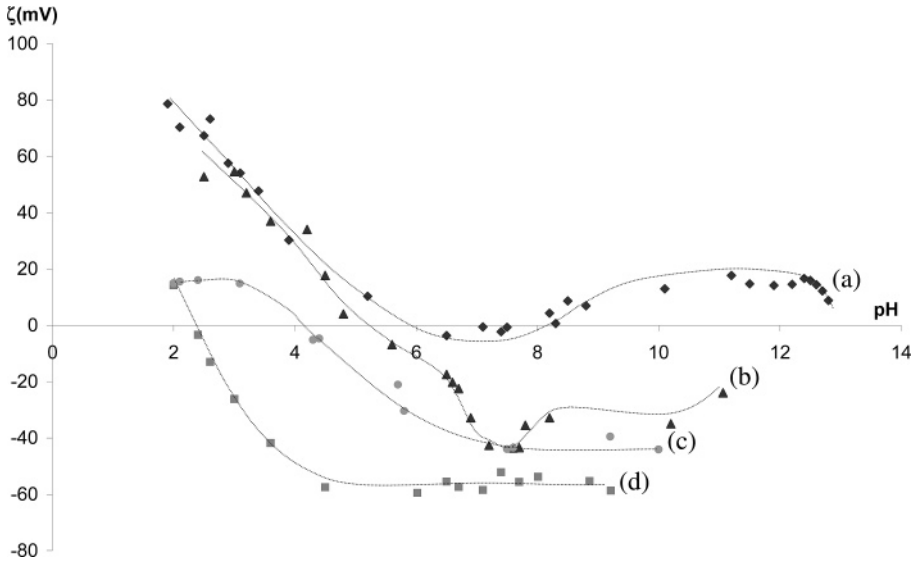

Figure 2. ζ potential as a function of pH of BST nanoparticles: (a) pristine BST nanoparticles; (b) HNO_3-treated BST nanoparticles; (c) citric acid treated BST nanoparticles; (d) BST@silica(25) nanoparticles.

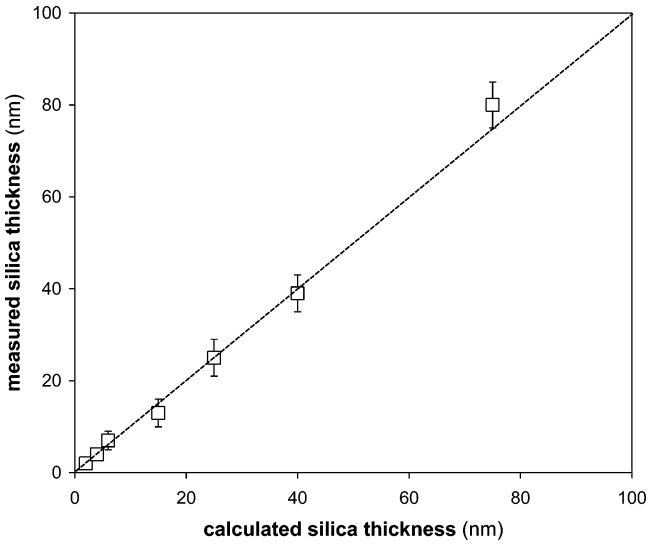

Figure 3. Thickness evolution of the silica shell as determined by TEM as a function of the calculated thickness according to eq 1.

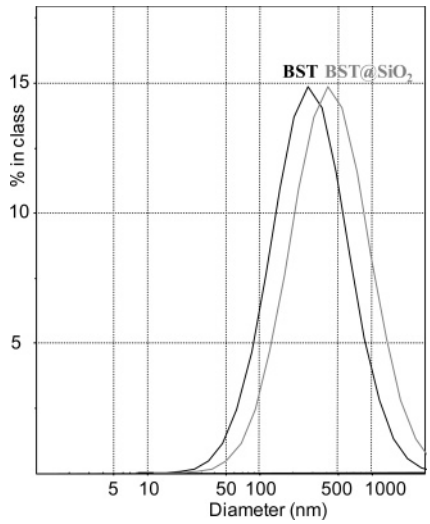

Figure 4. Size distributions of citric acid treated BST and raw BST@silica-(25) nanoparticles.

(25), equal to 2.4, confirms that all the BST particles have been surrounded by silica (Figure 2d). This result was confirmed by TEM experiments. Figure 1 displays the TEM pictures at various stages of the synthesis. As clearly evidenced in these pictures, the shell was homogeneous in size all around the particles, even at sharp edges. Furthermore, despite the polydispersity in size and shape of the BST particles, all of them were surrounded entirely by the same silica shell thickness. Finally, these TEM images demonstrated that the method used is very suitable for controlling the value of silica shell thickness. Indeed, the computed and experimental values of silica shell thickness for each stage of the synthesis are very close (Figure 3).

Size Sorting of BST@silica Nanoparticles. As already mentioned, the BST@silica nanoparticles presented a wide size distribution with a polydispersity index equal to 0.58 (Figure 4). To decrease this particle size distribution and extract the majority size of about 200 nm (corresponding to 150 nm expected BST cores added 50 nm of silica shell), a centrifugation procedure was carried out. It was based on the sedimentation rate of the particles and might be compared to a fractional distillation. Figures 5b and 5c display the BST@silica(25) nanoparticles as found in the supernatant (S1) and the pellet (P1) part after the first centrifugation, respectively. The efficiency of the first centrifugation is obvious: in the supernatant part, most of the little particles were removed and the size distribution in the pellet part was made narrower. This phenomenon was even more important after three stages of centrifugation (Figure 5d). This is confirmed by the value of the polydispersity index, i.e., 0.05 for P1 and 0.04 for P3. In Figure 5d, it may be observed that coated particles ordered themselves in a 2-D close packing, while they dried on the carbon film of the TEM grid. This spontaneous organization can only be observed for size-monodispersed core−shell particles.

Sintering of BST@silica Nanoparticles and Dielectric Behavior of the Resulting BST/Silica Composites. Dense compacts are required to use the core−shell particles for dielectric applications. As well-known in ferroelectric ceramics, residual porosity is highly detrimental for dielectric

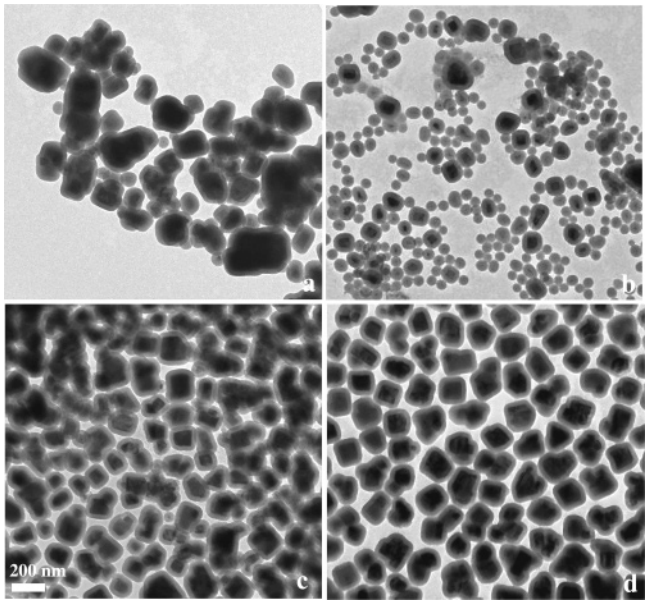

Figure 5. TEM pictures of (a) raw BST@silica(25) nanoparticles; (b) BST@silica(25) nanoparticles as obtained in the supernatant after the first centrifugation cycle (S1 product); (c) BST@silica(25) nanoparticles as obtained in the pellet after the first centrifugation cycle (P1 product); (d) BST@silica(25) nanoparticles as obtained in the pellet after the third centrifugation cycle (P3 product). (Scale bar 200 nm for all pictures.)

evaluation. The compacts were processed uniaxially pressing the starting powders presented in pellets and further sintering of the disks. For BST@silica, the sintering process is considered to be governed by the silica phase,[38] consequently reducing the sintering temperature compared to the one of pure BST (i.e., 1400 °C). Two parameters are of main relevance for the optimization of the final density: the porosity and the contact between cores. The objective is to keep the BST grains isolated in the final dense composite, the silica shell playing the role of dielectric loss barrier. The kinetics of matter transport depends on the characteristics of the initial green powder, the selected sintering temperature, and the uniformity and the thickness of the silica shell at the end of the sintering. Sintering at high temperature (1200 °C) favors the contact growth compared to the shrinkage since the first stage of the sintering. Moreover, a minimum initial silica thickness is necessary to obtain a complete densification before contact between the cores. But, from a dielectric point of view, a slight increase of the silica shell thickness leads to a strong decrease of the dielectric constant ($\epsilon'_{\text{silica}} \sim 4$). Thus, to obtain isolated ferroelectric particles and to keep sufficiently high permittivity, a compromise on the silica thickness in the starting core−shell particles has to be found. Low-temperature sintering would allow obtaining, by decreasing the porosity, a high enough density before the contact stage.

Preliminary attempts of sintering were performed on raw BST@silica(40). This sintering process consists of a heating treatment at 1050 °C for 6 h with two additional steps at 250 and 600 °C, which were determined from the thermogravimetric analysis and correspond to impurities removal (resulting from the initial soft chemistry route used). An approximate value of the composite relative density, ρ, close to 72% was obtained using

$$\rho = (\rho_{\text{core}} V_{\text{core}} + \rho_{\text{shell}} V_{\text{shell}})/(V_{\text{core}} + V_{\text{shell}}) \quad (2)$$

$$V_{\text{core}} = {}^4/_3 \pi r_{\text{core}}{}^3 \text{ and } V_{\text{shell}} = {}^4/_3 \pi [(r_{\text{core}} + r_{\text{shell}})^3 - r_{\text{core}}{}^3] \quad (3)$$

with $\rho_{\text{core}} = 5.6$ g/cm^3 and $\rho_{\text{shell}} = 2.27$ g/cm^3; $r_{\text{core}} = 75$ nm and $r_{\text{shell}} = 40$ nm.

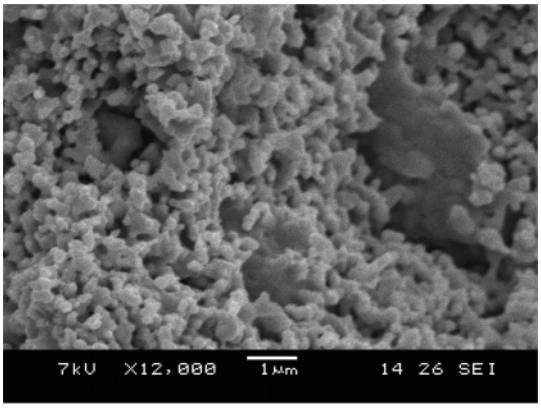

Figure 6. SEM micrographs of BST/silica composites as obtained after sintering at 1050 °C for 6 h of raw BST@silica(40) nanoparticles.

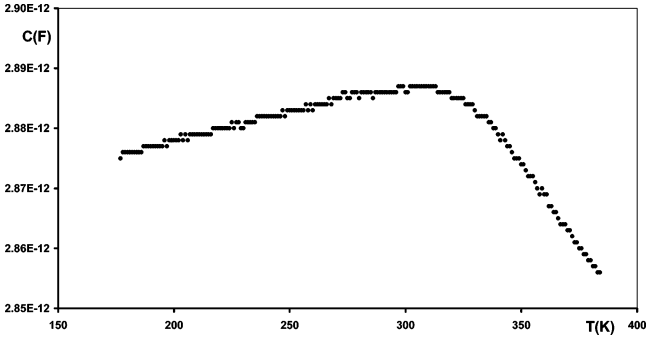

Figure 7. Capacitance versus temperature as measured at 100 kHz on sintered BST@silica(25) composite.

Figure 6 shows the SEM image of the fracture surface of BST/silica composite obtained through the sintering of raw BST@silica(40). The estimated average particle size is about 250 nm, indicating no grain growth at this sintering stage. An important porosity is observed in agreement with the low value of the density obtained which corresponds to an intermediate stage in sintering. Large well-densified regions (>1 μm) appear within the matrix composed of interconnected nanoparticles. This is the result of differential sintering due to agglomeration and particle size distribution in the green powder.

Dielectric measurements performed as a function of temperature at 100 kHz are shown in Figure 7. First of all, the transition temperature of pure BST ($T_c = 280$ K) was maintained in the BST/silica composite. This shows that the chemical interdiffusion between the core and the shell was very moderate, contrary to the standard composites obtained by solid state reaction for which the Curie temperature is usually lowered.[5] Both the porosity and the silica phase are responsible for the low values of the capacitance obtained which does not allow us to compute an effective dielectric permittivity. Because of the low sample relative density,

(38) Jagota, A. *J. Am. Ceram. Soc.* **1994**, *77*, 2237.

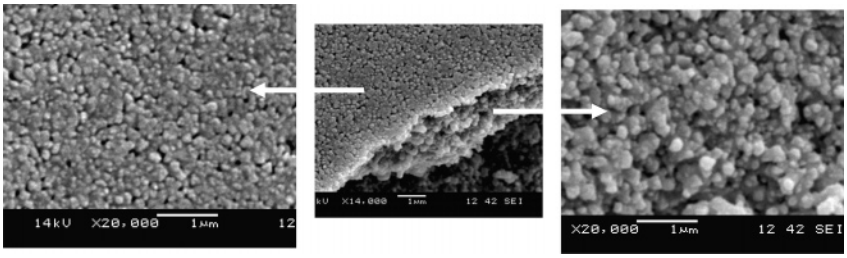

Figure 8. SEM micrographs of BST/silica composites as obtained after sintering at 1000 °C for 3 h of colloidal BST@silica(5) nanoparticles.

effective medium approximation mixing the dielectric permittivities of silica and of BST cannot be applied in this case. The dielectric losses at 100 kHz were negligible in the whole temperature range ($tg(\delta) \ll 0.001$), thus staying below the detection limit of our experimental setup. An increase of the sintering temperature, i.e., 1150 °C, leads rapidly to an abnormal grain growth. To overcome the limitations resulting from the sintering in normal conditions, the colloidal route was explored from the well-known silica opalline structures. The sintering process of 3-D periodic packing of nanometer-sized SiO_2 particles was studied (0.2−0.8 μm).[39] The formation of the necks starts around 800 °C through the viscous flow process and over 950 °C the morphology of the silica particles is changed by the development of the necks but long-range order is conserved.[40] A suspension of monodispersed nanoparticles, obtained via a size-sorted process, was used. Ordered arrangement of the ferroelectric core−shell was obtained by natural sedimentation of the suspension. This step allows one to obtain directly the greatest green compact compacity of 0.63 (value of the random compact packing fcc structure). Then the porosity was decreased by consolidation at a low sintering temperature. In considering the sintering path as a three-stages process,[41] which are particles rearrangement, densification, and grain growth, the use of initial colloidal packing powder presents several advantages. First, the step of compaction which generally leads, in the case of fine grains, to heterogeneous compaction with agglomerates and macroporosity is here avoided. Then the solid−solid interfaces are increased in sedimented particles, thus minimizing the energy associated with the rearrangement stage, leading, in the ideal case, to its removal. Furthermore, from a kinetic point of view, the densification stage arises more rapidly, i.e., at lower temperature. The last point of interest is that the final grain growth stage is then avoided. In light of the previous dielectric results, the silica shell thickness was reduced from 40 to 5 nm in order to increase the permittivity of the composite. Consequently, the thermal cycle was modified, taking into account the silica opals sintering conditions described in the literature: sintering performed in air at 1000 °C for 3 h with a relatively slow heating rate of 100 °C/h with the same two additional steps at 250 and 600 °C. SEM observations on both surface and fracture surface of the sample evidences a homogeneous microstructure and above all it confirms the formation of necks between the core−shell nanoparticles at such a low sintering temperature (Figure 8). This is not observed in the compacted powder sintered in the same conditions: the nanograins remain isolated. In this case, the stage reached in the sintering path is that of rearrangement and not yet that of matter diffusion.

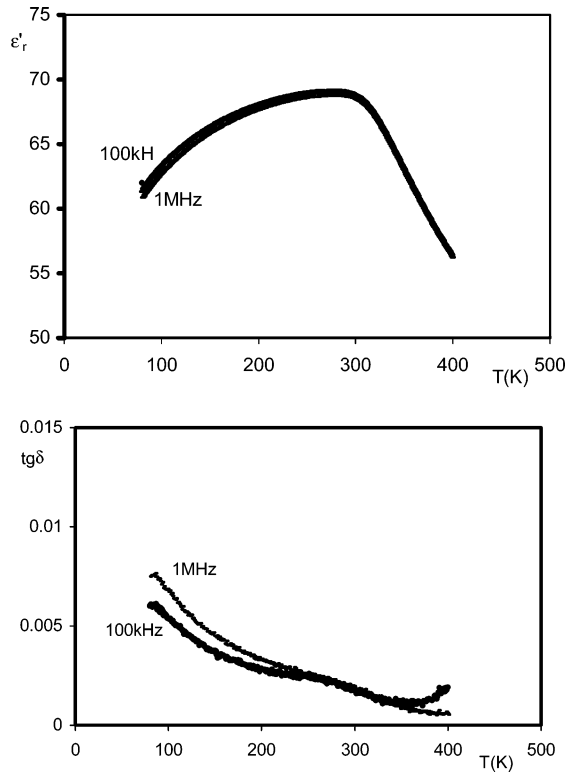

Figure 9. Dielectric permittivity and losses versus temperature measured at 100 kHz and 1 MHz on sintered colloidal BST@silica(5) composite.

Dielectric measurements performed on the calcined colloidal composite exhibits the expected properties. Noteworthy is the transition temperature remaining the same as the one of ferroelectric cores. Furthermore, the value of the dielectric permittivity reaches a reasonable value at room temperature for the aimed applications (eps'max = 70). And finally, the dielectric losses are much lower than the 1% limit and moreover remain very stable as a function of temperature (Figure 9).

Conclusion

A method based on a seeded growth procedure was modified to coat $(Ba_{0.6}Sr_{0.4})TiO_3$ ferroelectric nanoparticles with dielectric silica shell. The aim was to process new ferroelectric nanocomposite materials for telecommunication applications.

(39) Maroyal, R.; Requena, J.; Moya, J. S.; Lopez, C.; Cintas, A.; Miguez, H.; Meseguer, F.; Vazquez, L.; Holgado, M.; Blanco, A. *Adv. Mater.* **1997**, *9*, 257.
(40) Miguez, H.; Meseguer, F.; Lopez, C.; Blanco, A.; Moya, J. S.; Requena, J.; Mifsud, A.; Formes, V. *Adv. Mater.* **1998**, *10*, 481.
(41) Dupont, A. Thesis, University Bordeaux I, 2004.

To avoid contamination of the final composite material, citric acid was successfully selected as a stabilizing agent to improve the colloidal stability of BST particles in the ethanol reacting medium. The synthesis method allowed controlling accurately the silica shell thickness, as was the essential aim of this study. Indeed, the expected silica thickness matched the effectively coated one in the thickness range from a few nanometers to 100 nm. Both size sorting and washing were simultaneously performed, avoiding an additional step in the process.

First attempts of low-temperature sintering on compacted powder allowed obtaining BST/silica (40 nm) composite ceramics. The corresponding microstructure is heterogeneous due to the agglomeration of the green powder. However, the Curie temperature of the ferroelectric cores, which is an intrinsic parameter, is maintained in the composites. Such a result is hardly achieved in standard ferroelectric/dielectric composites. Capacitance and dielectric losses values nevertheless greatly decrease by the contribution of the silica phase. To improve both the microstructure and the dielectric performances, our strategy was to take advantage of the self-assembly properties of size-sorted BST@silica (5 nm) nanoparticles. SEM results have shown evidence of the neck formation at only 1000 °C. Reliable dielectric characterization was possible on as-calcined colloidal composites. The ferroelectric transition temperature was kept, the dielectric permittivity reached expected values, and the dielectric losses were very low and stable in the whole temperature range. This last result confirms that the silica shell acts as a dielectric loss barrier while keeping the intrinsic properties of the ferroelectric cores.

Acknowledgment. Stéphane Mornet is a recipient of a postdoctoral fellowship from the Conseil Régional d'Aquitaine.

CM050884R